

Introduction

Complex systems are typically heterogeneous as individuals vary in their properties, their response to the external environment, and to each other. In particular, many biological systems that show flocking involve self-propelled particles with heterogeneous interactions, which motivates the study of populations with multiple species. In this work, we consider the two-species variant of the Vicsek model [1] (TSVM) and the active Ising model [2] (TSAIM), consisting of two kinds of self-propelled particles that tend to align with particles from the same species and to antialign with the other. These two-species models show a flocking transition that is reminiscent of the original one-species model, as a liquid-gas phase transition, and display phase-separation in the coexistence region where dense liquid bands of each species propagate in a gaseous background. The interesting feature of these models is the appearance of two dynamical states in the coexistence region: the PF (parallel flocking) state in which all bands of the two species propagate in the same direction, and the APF (antiparallel flocking) state in which the bands of two different species move in opposite directions. PF and APF states perform stochastic transitions from one to the other only in TSVM, and the APF liquid phase of the TSVM is replaced by a high-density PF state in the TSAIM. We also study the impact of particle switching from one species to another.

Two-species Vicsek model (TSVM)

- ▶ N particles in a $L_x \times L_y$ periodic domain. Average density: $\rho_0 = N/L_x L_y$.
- ▶ Each particle carries a position $\mathbf{r}_i^t = (x_i^t, y_i^t)$, a spin-orientation $\sigma_i^t = (\cos \theta_i^t, \sin \theta_i^t)$ and a species-spin $s_i^t = \pm 1$ ($s_i^t = +1$ for an A particle and $s_i^t = -1$ for a B particle). We focus here on $N_A = N_B = N/2$.
- ▶ Time-evolution: $\theta_i^{t+1} = \langle \theta_i^t \rangle + \eta \xi_i^t$ and $\mathbf{r}_i^{t+1} = \mathbf{r}_i^t + v_0 \sigma_i^{t+1}$, with $\langle \sigma_i^t \rangle = \sum_{j \in \mathcal{N}_i} s_j^t \sigma_j^t$, and ξ_i^t scalar noise distributed uniformly in $[-\pi, \pi]$. $v_0 = 0.5$ if not specified.
- ▶ Order parameters: $\mathbf{v}_s(t) = \frac{1}{N} \sum_{i=1}^N \sigma_i^t = \mathbf{v}_+(t) + \mathbf{v}_-(t)$ and $\mathbf{v}_a(t) = \frac{1}{N} \sum_{i=1}^N s_i^t \sigma_i^t = \mathbf{v}_+(t) - \mathbf{v}_-(t)$.

TSVM: different states

- ▶ Two different states are observed: anti-parallel flocking (APF) and parallel flocking (PF) states.

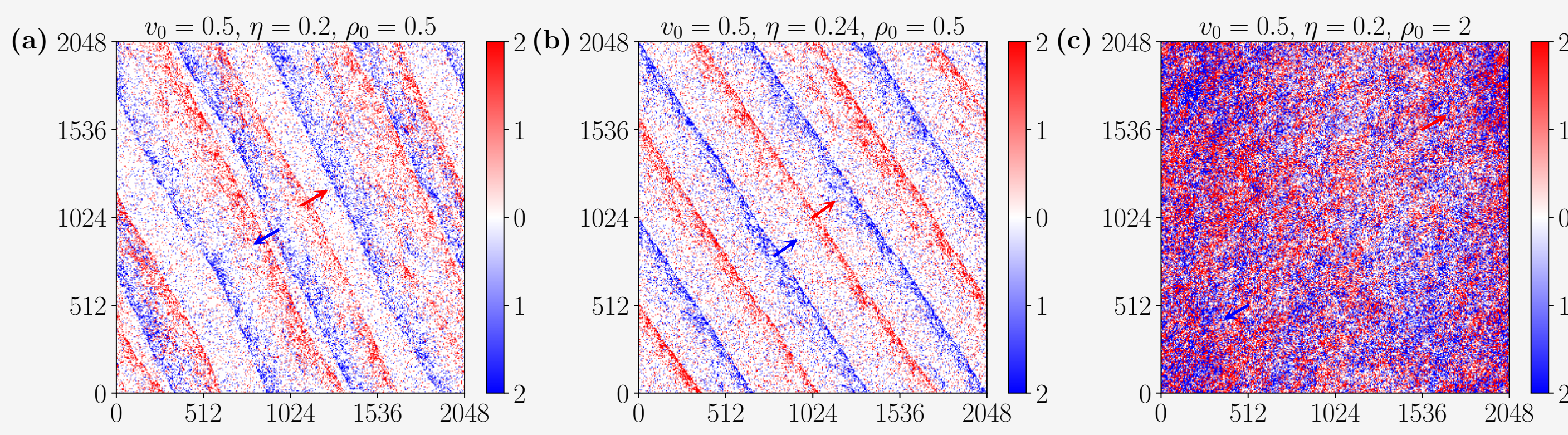
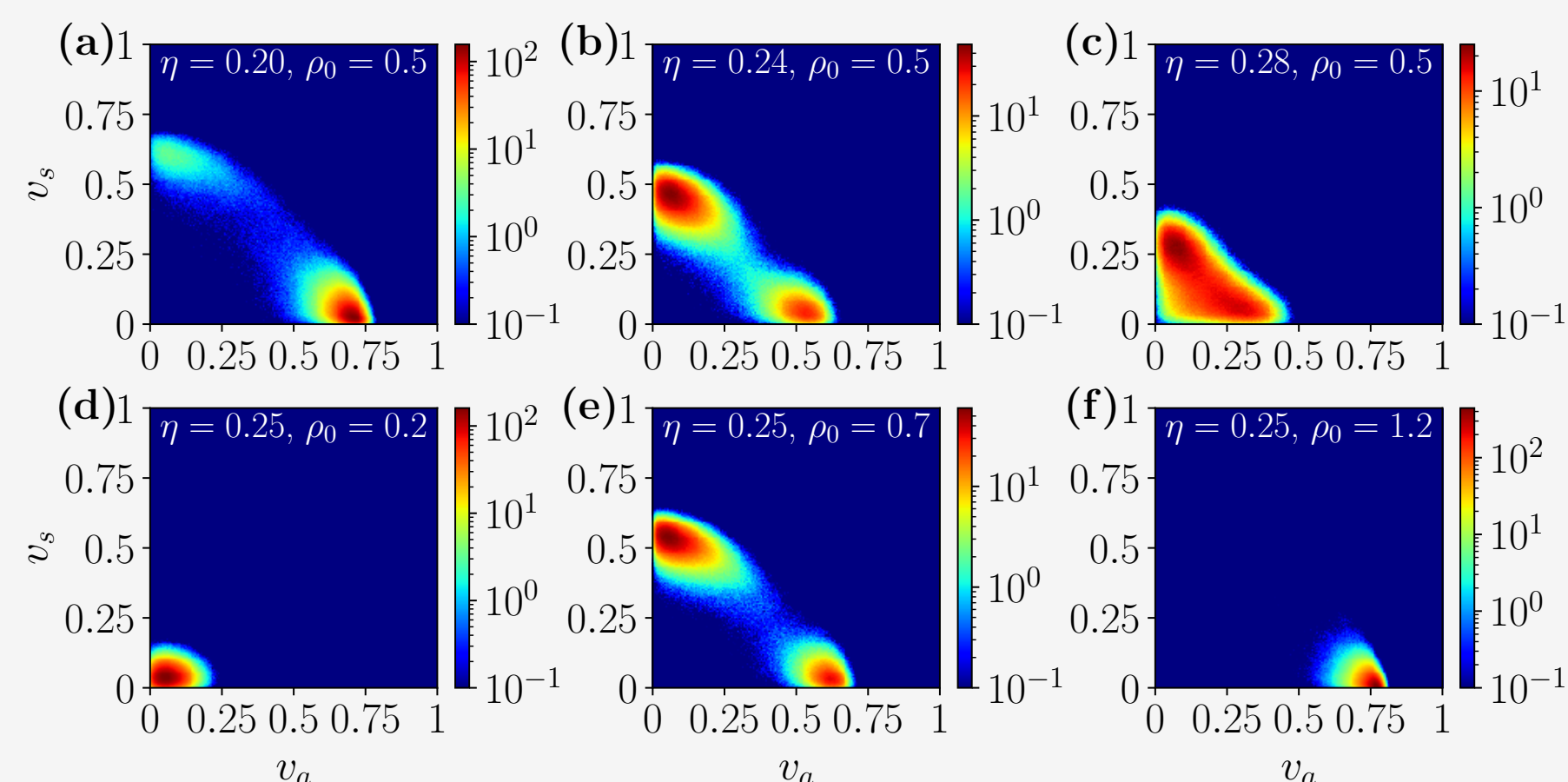
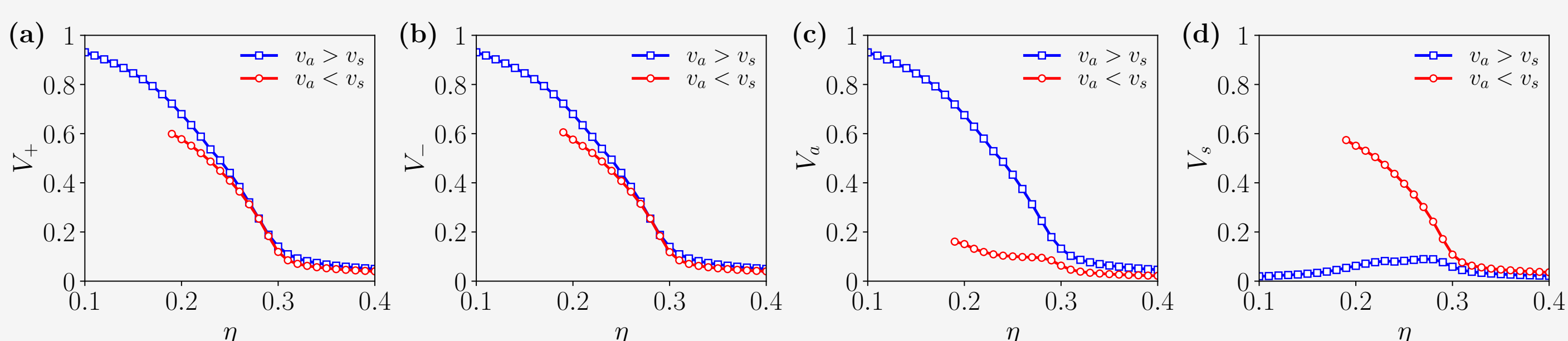


Fig. 1.1: (a) APF and (b) PF states in coexistence region. (c) APF liquid state.

TSVM: order parameters and states

- ▶ APF state means $v_a > v_s$ and PF state means $v_s > v_a$ (with $v_s = |\mathbf{v}_s|$, and $v_a = |\mathbf{v}_a|$).


 Fig. 1.2: Probability distribution $P(v_s, v_a)$. Two peaks indicate switching between the APF and PF states.

 Fig. 1.3: Order parameters $V_{\pm} = \langle |\mathbf{v}_{\pm}| \rangle$, $V_{s,a} = \langle v_{s,a} \rangle$ in the restricted APF and PF ensembles ($\rho_0 = 0.5$).

TSVM: phase diagrams

- ▶ Similarly to VM [1], the flocking transition is a liquid-gas phase transition.

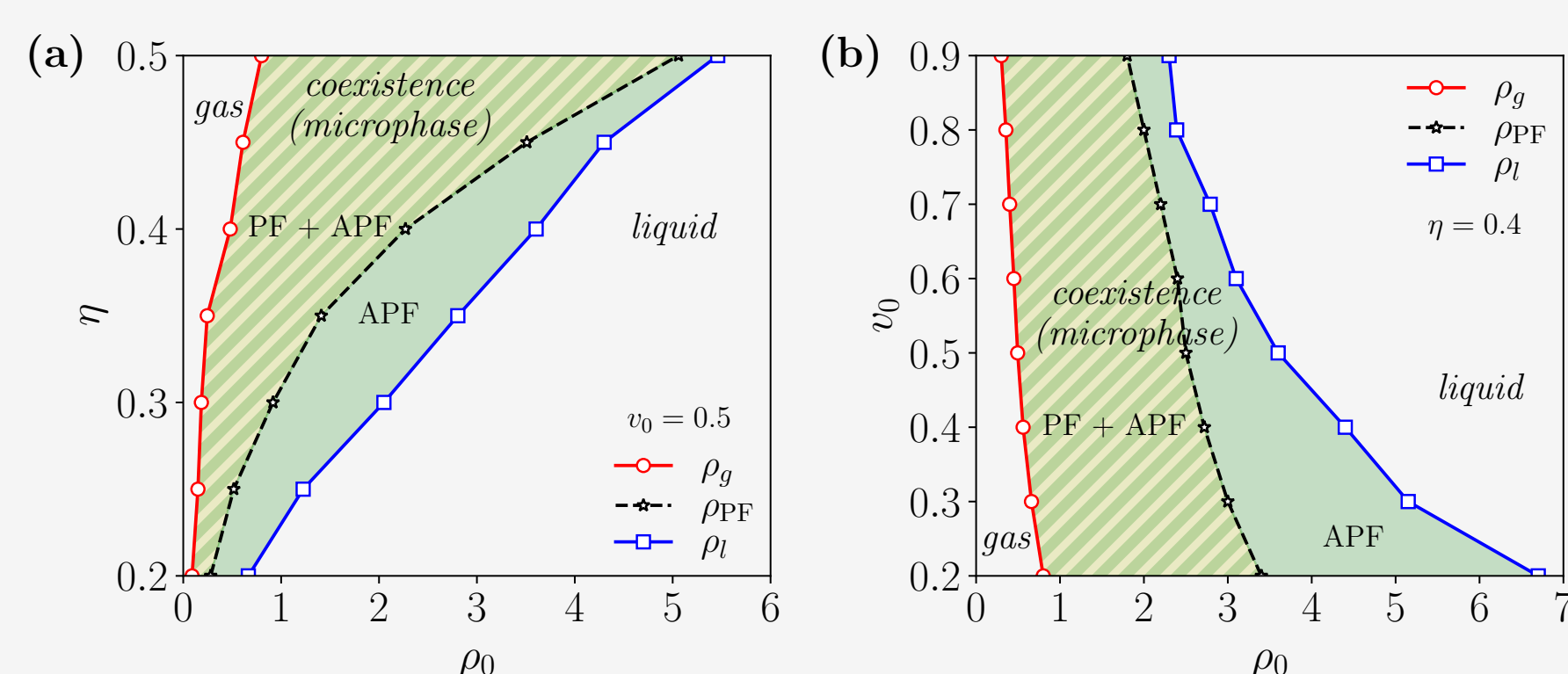
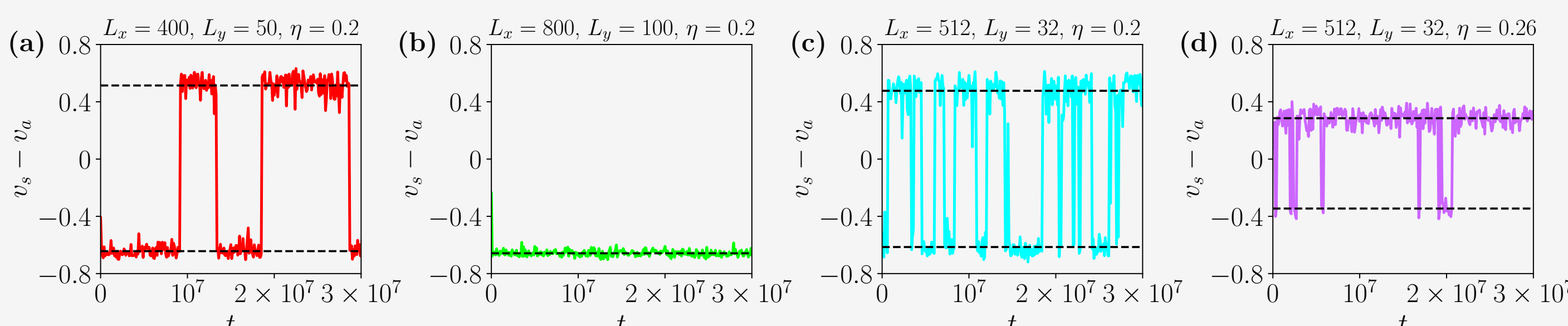
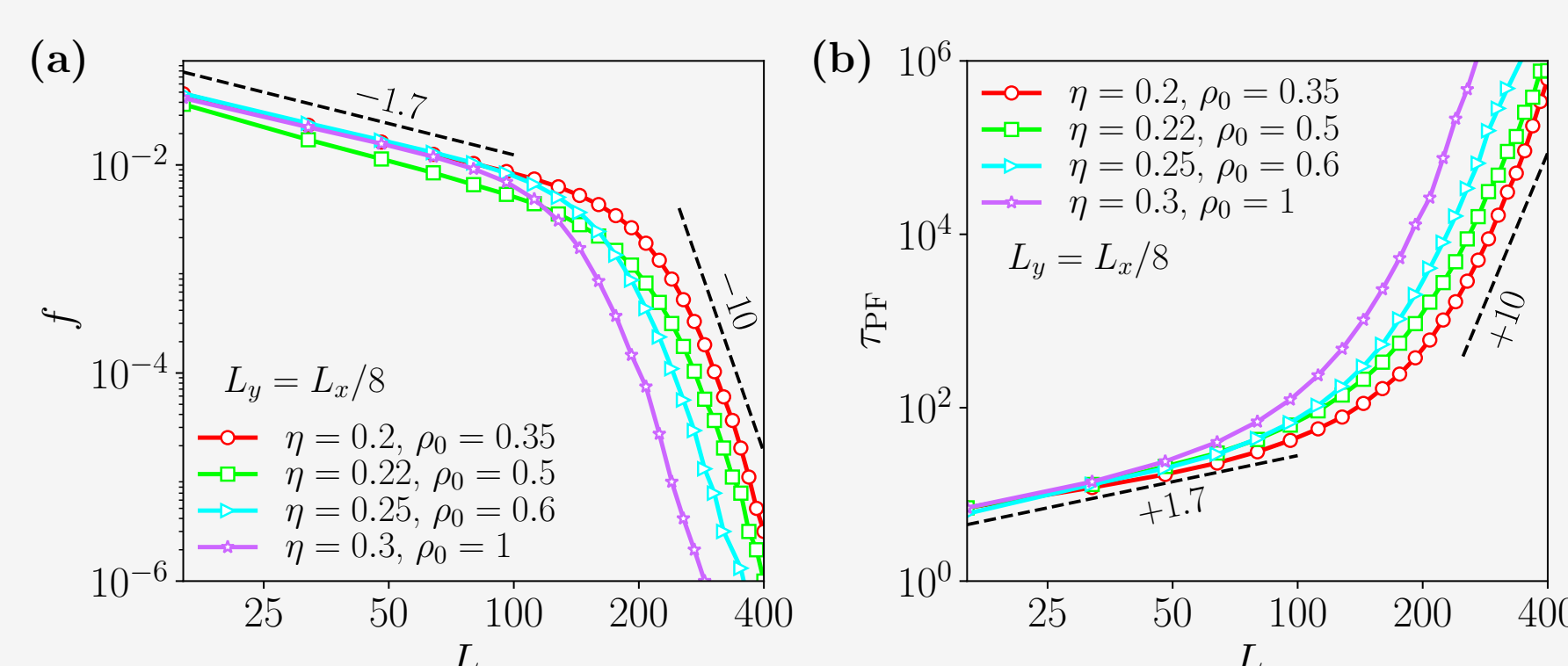


Fig. 1.4: (a) Noise-density phase diagram. (b) Velocity-density phase diagram.

TSVM: APF/PF transitions

- ▶ In the APF+PF region, the system switches stochastically between the APF and PF states.


 Fig. 1.5: Comparison of the time series of $v_s - v_a$ at two system sizes (a,b), and at two noise strengths (c,d).

 Fig. 1.6: (a) Average frequency f of APF/PF transitions. (b) Average time τ_{PF} spent in the PF state.

Two-species active Ising model (TSAIM)

- ▶ N particles on a $L_x \times L_y$ periodic lattice. Average density: $\rho_0 = N/L_x L_y$.
- ▶ j^{th} particle on site i carries a spin-orientation $\sigma_i^j = \pm 1$ and a species-spin $s_i^j = \pm 1$ ($s_i^j = +1$ for an A particle and $s_i^j = -1$ for a B particle). We focus here on $N_A = N_B = N/2$.
- ▶ Order parameters on site i : $v_{s,i} = \sum_{j=1}^{\rho_i} \sigma_i^j$ and $v_{a,i} = \sum_{j=1}^{\rho_i} s_i^j \sigma_i^j$, with ρ_i the number of particles on site i .
- ▶ Local Hamiltonian on site i : $H_i = -\frac{J}{2\rho_i} \sum_{j \neq k} (s_i^j \sigma_i^j)(s_i^k \sigma_i^k) = -\frac{J}{2\rho_i} v_{a,i}^2 + \frac{J}{2}$.
- ▶ Flipping rate: $W_{\text{flip}}(\sigma \rightarrow -\sigma) \propto \exp(-\beta \Delta H_i) = \exp\left(-\frac{2\beta J}{\rho_i} s \sigma v_{a,i}\right)$.
- ▶ Hopping rate in direction \mathbf{p} : $W_{\text{hop}}(\mathbf{p}, \sigma) = D(1 + \varepsilon \sigma \mathbf{p} \cdot \mathbf{e}_x)$.

TSAIM: different states

- ▶ APF and PF states are observed in the coexistence and liquid regions.

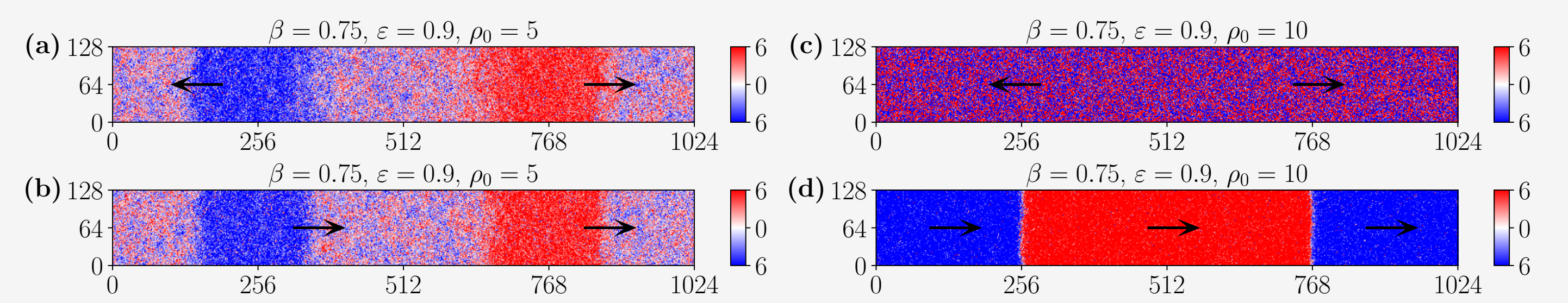
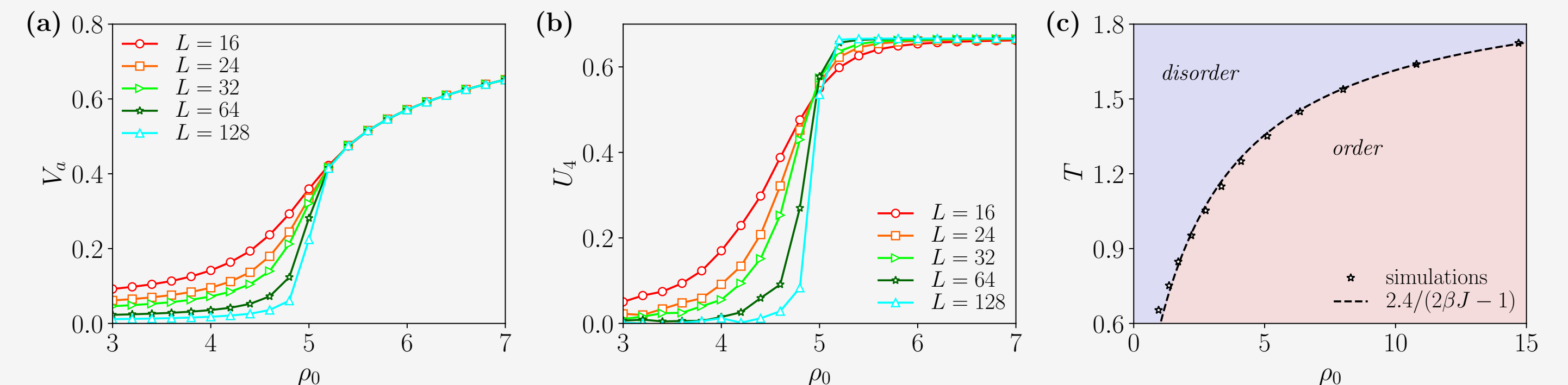


Fig. 2.1: (a) APF and (b) PF states in coexistence region. (c) APF liquid state. (d) PF high-density state.

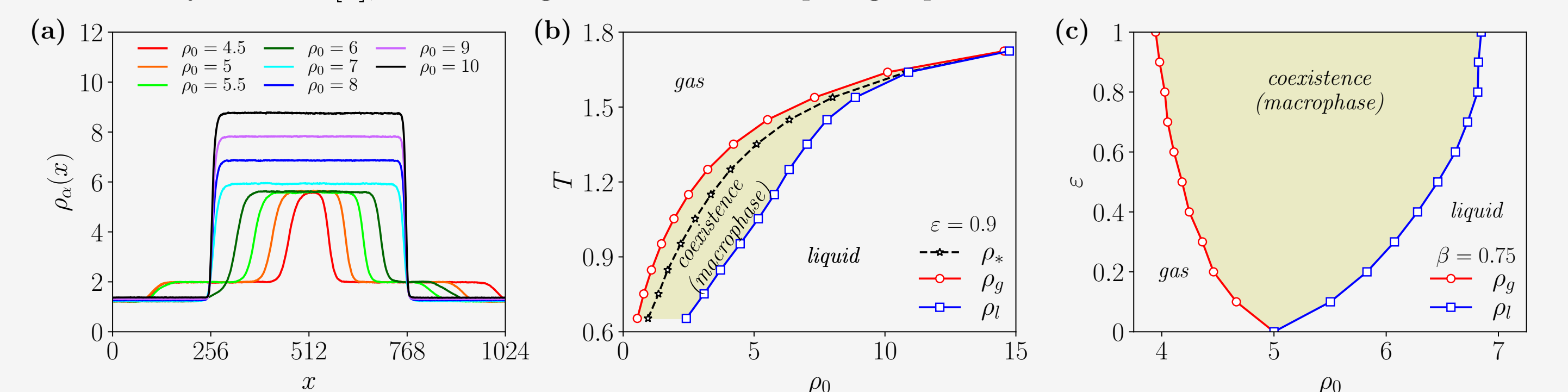
 TSAIM: $\varepsilon = 0$ phase transition

- ▶ $V_a = \langle v_a \rangle$ plays the role of order parameter when $\varepsilon = 0$, leading to a second order phase transition.


 Fig. 2.2: (a) Order parameter V_a and (b) Binder cumulant $U_4 = 1 - \langle v_a^4 \rangle / 3 \langle v_a^2 \rangle^2$ vs ρ_0 , for $\beta = 0.75$. (c) Temperature-density phase diagram.

TSAIM: density profiles and phase diagrams

- ▶ Similarly to AIM [2], the flocking transition is a liquid-gas phase transition.


 Fig. 2.3: (a) Density profiles for increasing density, $\beta = 0.75$, $\varepsilon = 0.9$. (b) Temperature-density phase diagram. (c) Velocity-density phase diagram.

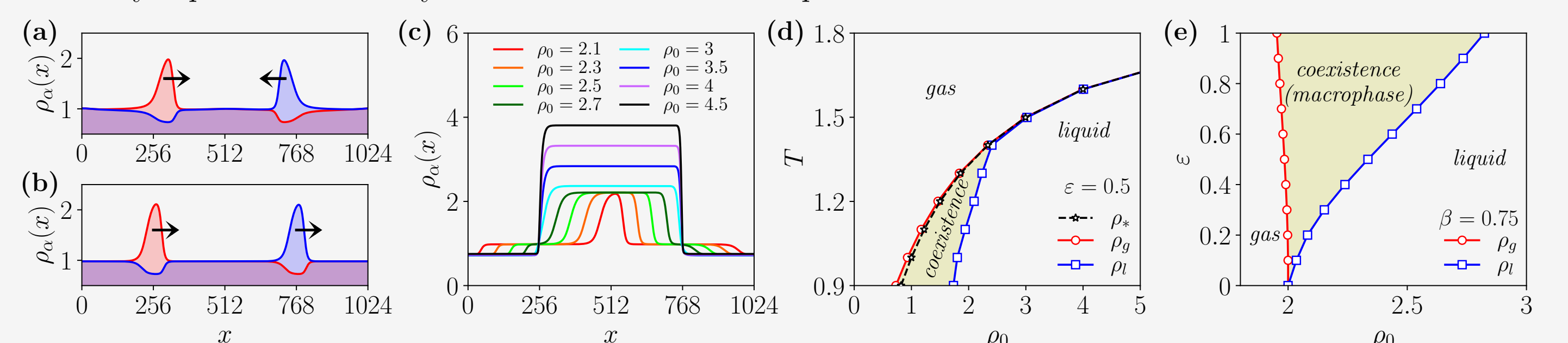
TSAIM: hydrodynamic description

- ▶ Hydrodynamic equations for $\rho = \rho_A + \rho_B$, $m = \rho_A - \rho_B$, $v_s = m_A + m_B$, $v_a = m_A - m_B$:

$$\begin{aligned} \partial_t \rho &= D \nabla^2 \rho - v \partial_x v_s, & \partial_t m &= D \nabla^2 m - v \partial_x v_a, \\ \partial_t v_s &= D \nabla^2 v_s - v \partial_x \rho - 2 \left(1 + \frac{r'}{\rho} + 3\kappa \frac{v_a^2}{\rho^2} \right) v_s + 4\beta J \left(1 + \frac{r'}{\rho} + \kappa \frac{v_a^2}{\rho^2} \right) \frac{m v_a}{\rho}, \\ \partial_t v_a &= D \nabla^2 v_a - v \partial_x m + 2 \left(2\beta J - 1 - \frac{r}{\rho} - \alpha \frac{v_a^2}{\rho^2} \right) v_a, \end{aligned}$$

with $v = 2D\varepsilon$, $\kappa = 2(\beta J)^2/3$, $\alpha = 2(\beta J)^2(1 - 2\beta J/3)$, and $r = (3 - 2\beta J)r'$.

- ▶ They reproduce correctly the behavior of microscopic simulations.


 Fig. 2.4: (a) APF and (b) PF states, for $\beta = 0.75$, $\varepsilon = 0.9$, $\rho_0 = 2.05$. (c) Density profiles for increasing density, $\beta = 0.75$, $\varepsilon = 0.9$. (d) Temperature-density phase diagram. (e) Velocity-density phase diagram.

References

- [1] T. Vicsek, A. Czirok, E. Ben-Jacob, I. Cohen and O. Shochet, Phys. Rev. Lett. **75**, 1226 (1995).
- [2] A. P. Solon and J. Tailleur, Phys. Rev. Lett. **111**, 078101 (2013); Phys. Rev. E **92**, 042119 (2015).
- [3] S. Chatterjee, M. Mangeat, C.-U. Woo, H. Rieger, and J. D. Noh, Phys. Rev. E **107**, 024607 (2023).

Acknowledgements

SC, MM and HR were financially supported by the German Research Foundation (DFG) within the Collaborative Research Center SFB 1027-A3 and INST 256/539-1. JDN acknowledges the computing resources of Urban Big data and AI Institute (UBAI) at the University of Seoul.